

Dislocations and the commensurate-incommensurate transition in two dimensions

S. N. Coppersmith* and Daniel S. Fisher
Bell Laboratories, Murray Hill, New Jersey 07974

B. I. Halperin
Physics Department, Harvard University, Cambridge, Massachusetts 02138
and Bell Laboratories, Murray Hill, New Jersey 07974

P. A. Lee and W. F. Brinkman
Bell Laboratories, Murray Hill, New Jersey 07974

(Received 17 August 1981)

The stability of weakly incommensurate two-dimensional solid phases described by periodic arrays of discommensurations has been investigated. It is shown that incommensurate phases consisting of a small number of possible commensurate domains of either the striped or honeycomb type are unstable with respect to the spontaneous creation of dislocations. Such phases are consequently "liquids," with exponential decay of correlations. The consequences of these results on the phase diagram of overlayers and the relation with experiment is discussed.

I. INTRODUCTION

Rare-gas atoms and other molecules absorbed on graphite exhibit a wide variety of commensurate and incommensurate phases that are two dimensional in nature.¹ One of the questions of considerable theoretical interest is the nature of the phase transition between commensurate and incommensurate phases (*C-I* transition). Perhaps the most extensively studied example is the *C-I* transition from the Kr $\sqrt{3} \times \sqrt{3} R 30^\circ$ commensurate phase.^{2,3} This transition has been considered to be a continuous transition in that the difference between the commensurate reciprocal-lattice vector and the incommensurate lattice vector appears to go to zero as the $\frac{1}{3}$ power of the chemical potential difference between the two phases.⁴

Recently, however, it was shown that the transition may, in fact, be weakly first order and that the Bragg reflections broaden in proportion to their distance from the commensurate position.² It appears, therefore, that there is considerable disorder in the incommensurate phase.

The theoretical interest in this transition stems from the fact that as the difference between the reciprocal-lattice vectors of the substrate (\vec{G}) and adsorbate (\vec{H}) become small, one expects the coupling between the adsorbate and the substrate to induce a set of *discommensurations* or *domain walls* separating large commensurate regions such that the distance between domain walls is large compared to the width of the walls. In this regime much of the physics is independent of the microscopic interactions. As discussed by McMillan⁵ and by Bak and Emery,⁶ the *C-I*

transition at zero temperature for a one-dimensional array of such walls is expected to be second order because of the repulsive interaction between the discommensurations. A two-dimensional incommensurate system such as Kr on graphite could have walls in three directions because of its hexagonal structure. However, if intersections between the walls are energetically unfavorable, one expects instead a "striped" phase which has walls in only one direction. Such one-dimensional walls would strongly fluctuate about their equilibrium positions. Pokrovski and Talapov⁷ and Luther⁸ showed that these fluctuations contribute to the wall free energy and cause an effective repulsive interaction between walls that varies as $1/l^3$ where l is the average distance between walls. This repulsive interaction between the walls makes the *C-I* transition to the striped phase continuous.

Recently, Villain⁹ pointed out that a honeycomb array of walls has a degeneracy in that one can expand or contract the hexagons of the array without changing the total wall length or the number of nodes, as shown in Fig. 1. Since the wall length and number of nodes define the total energy of the system for well separated walls, Villain argued that this additional degeneracy leads to an entropy which when included in the free energy stabilizes the honeycomb phase relative to the striped phase and, in addition, causes the *C-I* transition to become first order.

The purpose of this paper is to examine the nature of the weakly incommensurate phases. Since both the striped phase and the honeycomb phase are incommensurate, they are two-dimensional solids which exhibit algebraic long-range order. However,

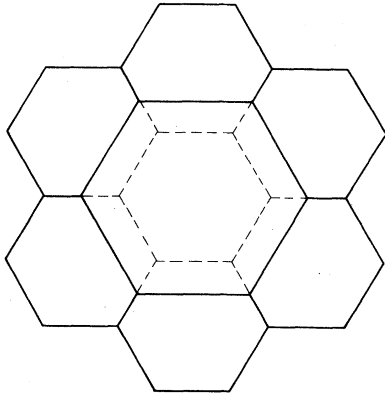


FIG. 1. "Breathing" freedom that contributes to entropy of honeycomb phase.

the elastic constants associated with the wall fluctuations need not be sufficient to stabilize these solids against spontaneous creation of dislocations. If this is the case, the $C-I$ transition must either take a commensurate solid to an "incommensurate liquid," or else the transition must be a "large" first-order transition which bypasses entirely the region where the domain walls are nonoverlapping. Using the Kosterlitz-Thouless theory^{10,11} for dislocation melting, we show that the stability criteria is temperature independent and that sufficiently near to low-order commensurate phases such as the $\sqrt{3} \times \sqrt{3} R 30^\circ$ phase of Kr on graphite, the incommensurate phase is unstable to dislocations.

In Sec. II, we examine rectangular phases which are incommensurate in one direction only. Using the results of Schulz¹² and Pokrovsky and Talapov,⁷ it is shown that if the number of different commensurate domains is p , then the weakly incommensurate striped phase can be stable only if $p \geq \sqrt{8}$. In Sec. III, we examine the honeycomb array of walls. The elastic constants of this phase are calculated from considerations of changes of the entropy due to strains and from numerical calculations of the displacement correlation functions. Here, we find that for adsorbate layers with N different possible commensurate domains arranged in a honeycomb array, the solid is stable only if $N \geq 7.5 \pm 1.5$.

In Sec. IV, we consider the question of a transition from the hexagonal-honeycomb arrays to the striped phase and discuss the effect of small rotations of the overlayer lattice due to the instability of Novaco and McTague.¹³ Finally, in the last section, we consider the possible relation of our work to the experiments on Kr absorbed on graphite and in addition, the consequences of this work with respect to the general phase diagram of overlayers.

The principal results of the present paper were reported earlier in a short letter by the authors.¹⁴ The

result for the breakdown of the Luther-Pokrovsky-Talapov theory due to dislocations, in the uniaxial case for $p < \sqrt{8}$, was found independently by Villain and Bak.¹⁵ In another independent work, Chui¹⁶ predicted that a softening of the elastic constants would cause a dislocation instability near the commensurate-incommensurate transition, for both the uniaxial and hexagonal cases. We disagree, however, with Chui's statement that the coefficient of the logarithmic interaction between dislocations in the incommensurate solid will vanish as the domain-wall separation goes to infinity.¹⁶ Rather, we find that the coefficient remains finite, and stability depends on the order of commensurability.

The importance of investigating the interplay between dislocation formation and the commensurate-incommensurate transition was emphasized by Villain.¹⁷

II. RECTANGULAR COMMENSURATE SOLIDS

For definiteness, we will first consider atoms adsorbed on a rectangular substrate with lattice constants a and c in the x and y directions, respectively. At some temperature T , we will assume that there is a range of chemical potential, ζ , for which the adsorbate forms a rectangular commensurate solid with lattice constants pa and c , i.e., a $p \times 1$ registered phase. There are thus p possible positions of the adsorbate lattice relative to the substrate; in the registered phase only one of the p domains will be present.

As the chemical potential is raised, the surface density of adsorbate atoms will increase. This may initially occur via interstitials or second layer promotion. We will, however, assume that above a critical value of the chemical potential, ζ_0 , it becomes energetically favorable for the adsorbate to form all p possible domains rather than just one. The resulting structure will be an incommensurate "striped" phase with the domains arranged sequentially in the x direction with the adsorbate atoms in each domain shifted, (on average) by $(np - 1)a$ (n an integer) with respect to those in the previous domain. This arrangement has the effect of adding $1/p$ of an extra row of atoms in the y direction at each domain wall. The x lattice constant of the adsorbate will hence be $pa(1 - a/l)$ where l is the average distance between domain walls.

There is a repulsive interaction between the walls which for low temperatures and l large has the value, per unit length of wall,⁹

$$\epsilon_{\text{int}} = C_1 \frac{V^{xx}(0)}{\kappa} e^{-\kappa l},$$

where C_1 is a positive constant, $V^{xx}(0)$ is the x curvature of the substrate potential at its minimum, and

$$\kappa^2 = \frac{V^{xx}(0)}{Y_0 pac}, \quad (2.1)$$

with Y_0 the microscopic Young's modulus of the adsorbate.⁹ At zero temperature, the domain walls form a regular parallel array with l determined by minimizing the free energy per unit area

$$f = \frac{\epsilon_w}{l} - \frac{\zeta}{lpc} + \frac{\epsilon_{\text{int}}(l)}{l}, \quad (2.2)$$

where ϵ_w is the energy per unit length of one wall, and ζ is the chemical potential. At $T=0$, the density of walls is hence $1/l \propto -\kappa \ln(\zeta - \epsilon_w pc)$ as ζ tends to the critical value, $\epsilon_w pc$.

At any nonzero temperature, however, the walls will no longer be straight—they will meander. For a single wall this will give rise to an entropic term which must be included in the free energy of the wall per unit length. At long wavelengths, the Hamiltonian of a single wall has the form

$$H_w = \int dy \left[\epsilon_w + \frac{\Gamma}{2} \left(\frac{dx}{dy} \right)^2 \right], \quad (2.3)$$

where the wall position is given by $x(y)$ and $\Gamma = \Gamma(T)$ is a stiffness coefficient for the wall which will be determined by the microscopic interactions and will be exponentially large at low temperatures, $\Gamma \propto \exp(\epsilon_m/T)$ due to the activation energy of microscopic kinks in the wall. Integrating over all the wall positions will give rise to a contribution to the free energy per unit length and to fluctuations in the x position of the wall

$$\langle [x(y_1) - x(y_2)]^2 \rangle = \frac{T|y_2 - y_1|}{\Gamma}. \quad (2.4)$$

The quantity T/Γ thus acts like a “diffusion” constant for the wall.

The fluctuations in the wall positions yield an effective entropic repulsion between the walls due to wall “collisions.” If the walls were distinguishable and could cross freely, then the total free energy of N walls separated on average l would just be N times the free energy of a single wall. However, every time two walls cross there is an indistinguishable configuration in which the two walls collide at the crossing points but do not cross. Therefore, there is a factor of 2 overcounting of the number of wall configurations according to whether or not they cross. It is thus necessary to subtract $\ln 2$ from the entropy (obtained if the walls were free) for each wall-wall collision. This yields a positive contribution to the free energy per unit area of the form

$$\Delta f_{\text{collisions}} = C_2 \frac{T^2}{\Gamma l^3} \quad (2.5)$$

(where C_2 is a constant).

This dominates the exponential repulsion between walls (ϵ_{int}), at any nonzero temperature for l sufficiently large. The free energy per unit area for l large

is thus

$$f = \frac{\zeta_0 - \zeta}{lpc} + \frac{C_2 T^2}{\Gamma l^3}, \quad (2.6)$$

where the free energy per unit length of one wall has been lumped into ζ_0 . For $\zeta > \zeta_0$, the free energy of the walls, Eq. (2.6), has a minimum at the equilibrium value of $l \propto (\zeta - \zeta_0)^{-1/2}$ as $\zeta \rightarrow \zeta_0$. Within this approximation of meandering infinitely long walls, the striped C - I transition can thus be second order with no jump in the lattice constant. The above estimates can be made more precise via a mapping of the problem onto a system of fermions in one dimension, as was done originally by Luther, Pokrovsky, and Talapov.^{7,8}

We now consider the properties of a weakly incommensurate striped phase in the limit of large l . From the above discussion it is easy to see that the array of meandering walls in the weakly incommensurate phase will have a resistance to bending in the y direction due to the wall stiffness Γ and a resistance to compression in the x direction due to the entropic repulsion. (The chemical potential will fix the average separation only.) Suppose \tilde{u}_i is the x displacement of the i th wall from its equilibrium position. For fluctuation wavelength much greater than l we can replace the discrete index i by the continuum variable x and define the displacement $\tilde{u}(x, y)$. The long-wavelength fluctuating part of the wall free energy per unit volume is

$$F = \frac{1}{2} \int d^2 r [\tilde{K}_x (\partial_x \tilde{u})^2 + \tilde{K}_y (\partial_y \tilde{u})^2], \quad (2.7)$$

where

$$\tilde{K}_y = \Gamma/l \quad (2.8)$$

and

$$\tilde{K}_x \propto \frac{T^2}{\Gamma l^3} = \frac{T^2}{\tilde{K}_y l^4} \quad (2.9)$$

are the elastic constants of the system of walls. We have assumed here that the displacements vanish at the boundaries of the sample, or that we have periodic boundary conditions, so there is no term proportional to $\nabla \cdot \tilde{u}$.

The wall free energy Eq. (2.7) can be simply related to the coarse-grained elastic free energy of the adsorbate. In the striped incommensurate phase, the y displacements, u_y , of the atoms from their average incommensurate positions will be small and non-divergent due to the registry in the y direction. The x displacements, $u = u_x$, will, on the other hand, fluctuate as the walls meander. At long wavelengths u can be simply related to the wall displacements: $-u = a\tilde{u}/l$, since u jumps by $-a$ at each wall. We hence conclude that

$$F = \frac{1}{2} \int d^2 r [K_x (\partial_x u)^2 + K_y (\partial_y u)^2], \quad (2.10)$$

where the adsorbate elastic constants are $K_{x,y} = \bar{K}_{x,y} l^2 / a^2$, so that as $l \rightarrow \infty$, $K_x \propto l^{-1}$ and $K_y \propto l$. A free energy of the form Eq. (2.10) is equivalent to an anisotropic x - y model. Long-wavelength fluctuations will yield power-law divergences in the structure factor characteristic of a two-dimensional floating solid. For \bar{q} near the incommensurate Bragg points \bar{G} , or near $\bar{G} + \bar{H}$ (with \bar{H} a substrate reciprocal-lattice vector) $S(\bar{q})$ will be anisotropic

$$S(\bar{q}) \sim \frac{1}{|K_x(q_x - G_x - H_x)^2 + K_y(q_y - G_y - H_y)^2|^{1-1/2\eta_G}}, \quad (2.11)$$

where the exponent $\eta_G = G_x^2 T (K_x K_y)^{-1/2} / 2\pi$ depends only on G_x . For the reciprocal-lattice vector, G_0 , with the smallest x component, $G_x = 2\pi/pa$ and hence $\eta_{G_0} = A/p^2$ where A is a constant independent of T , Γ , or l .

Schulz¹² has calculated the correlation function exactly in the limit of large l by mapping the statistical mechanics of the walls onto a one-dimensional fermion problem. He finds that $\eta_{G_0} = 2/p^2$, i.e., $A = 2$.

This implies that

$$\frac{a^2(K_x K_y)^{1/2}}{T} = \pi \quad (2.12)$$

in agreement (up to the previously undetermined constant) with the rough estimate of K_x above.

Kosterlitz and Thouless (KT)¹⁰ have shown that any system with a free energy of the form Eq. (2.10) will be unstable to free "vortices" above a critical temperature, T_{KT} . In this case the role of the vortices will be played by dislocations having Burgers vector in the x direction with magnitude pa —i.e., the minimal Burgers vector with $b = b_x$. The KT criterion for stability of the floating solid phase is

$$\frac{p^2 a^2 (K_x K_y)^{1/2}}{8\pi T} = \frac{p^2}{8} > 1. \quad (2.13)$$

We hence conclude that for $p = 2$ a sufficiently weakly incommensurate striped phase will be unstable to the presence of free dislocations and hence a fluid at any finite temperature.

Microscopically, each dislocation (independent of p) will be simply a rather distorted extra half row of atoms in the y direction ending at a point. However, it is instructive to also consider a dislocation in terms of the superlattice of walls. Since each wall includes $1/p$ of an extra row of atoms, a dislocation must consist of p half-walls ending at a point. Macroscopically, this is the smallest number of walls that can end at a point and still preserve the labeling $(1, 2, \dots, p)$ of the domains as shown in Fig. 2, for $p = 3$. The KT stability criterion Eq. (2.13) could have alternatively been derived in terms of the wall free energy Eq. (2.7) and wall elastic constants, $\bar{K}_{x,y}$ by considering

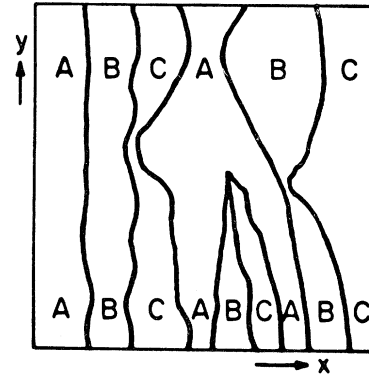


FIG. 2. Dislocation in a 3×1 rectangular incommensurate phase domain wall configuration.

the instability to a p -wall dislocation in the wall lattice with Burgers vector $B = pl$. In terms of this picture it is easy to see physically how p enters the stability criterion: the free energy of a p -wall dislocation is proportional to p^2 .

So far we have assumed that the wall elastic constants \bar{K}_x and \bar{K}_y entering Eq. (2.7) and the stability criterion, are simply given by Eqs. (2.8) and (2.9). This is not correct in general. Firstly, for any fixed l , at sufficiently low temperatures (or small l at any fixed temperature) the exponential wall repulsions will dominate over the entropic repulsion. This crossover will occur when $T \sim \epsilon_m / \kappa l$. Below this temperature, \bar{K}_x and \bar{K}_y will both increase and the system will solidify even for $p = 2$. The width in chemical potential, $\Delta\zeta$, of the fluid phase for $p = 2$ will be exponentially narrow at low temperatures, $\Delta\zeta \sim \exp(-\epsilon_m/T)$.

The second effect which will change \bar{K}_x and \bar{K}_y is the presence of dislocation pairs. Dislocations will generally decrease the elastic constants at long wavelengths. If there are free dislocations then the elastic constants will be renormalized to zero, causing the KT transition to a fluid state. However, if all the dislocations are in bound pairs, then the renormalized $\bar{K}_{x,y}$ will be nonzero. For this to occur, the renormalized infinite wavelength elastic constants must satisfy the KT stability criterion Eq. (2.13); if they do not, the system will melt. The renormalizations due to dislocation pairs may be sufficient to cause the $p = 3$ weakly incommensurate solid to melt at intermediate temperatures, resulting in a dip in the floating solid-fluid melting curve as shown in Fig. 3(a). However, at low temperatures the number of dislocation pairs will be thermally activated and hence exponentially small. The renormalized elastic constants will thus approach their "bare" values for large l ; and be larger than their bare values due to wall-wall interactions (see above) for smaller l . Therefore, the fluid phase should extend down to $T = 0$ only for

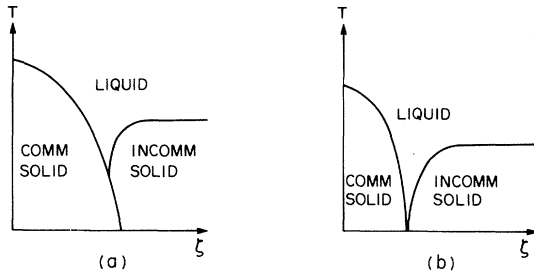


FIG. 3. (a) Possible phase diagram for 3×1 rectangular adsorbate. (b) Proposed phase diagram for 2×1 rectangular adsorbate.

$p < \sqrt{8}$, i.e., $p = 2$, as in Fig. 3(b).

The line separating the $p = 2$ commensurate solid from the liquid phase, which extends down to $T = 0$, represents a broken-symmetry transition with the two possible domains characteristic of the Ising model. It is probable that this transition is second order, in which case the transition should have the exponents of the two-dimensional Ising model. Thus, as one approaches the commensurate-liquid transition from either side, one should observe a correlation length ξ which diverges as $|\zeta - \zeta_c|^{-1}$, while the specific heat and the compressibility (defined as the derivative of the density of adatoms with respect to chemical potential) should diverge as $-\ln|\zeta - \zeta_c|$.

If the dislocation core energy is large, so that the density of dislocations is small, there should be a region inside the liquid phase, further from ζ_c , where the Luther-Pokrovsky-Talapov analysis gives the dominant contribution to the thermodynamic quantities. In this region, the specific heat and compressibility should vary as $(\zeta - \zeta_c)^{-1/2}$. The structure factor $S(\bar{q})$ should have well-defined maxima, displaced from the commensurate points by an amount $\delta \propto (\zeta - \zeta_c)^{1/2}$. The width of the peaks, or the inverse correlation length, is determined by the density of dislocations, whose behavior has not been analyzed in this regime.

At a higher value of the chemical potential ζ_i there will be a transition between the fluid and the incommensurate, or floating solid. If this phase transition is of the Kosterlitz-Thouless form, then the correlation length will diverge as $\exp[\text{const}/(\zeta_i - \zeta)^{1/2}]$, as the transition is approached.

III. FREE ENERGY FOR HONEYCOMB ARRAY

In this section we consider the commensurate-incommensurate transition for adsorbates on a hexagonal substrate such as graphite. Letting a be the lattice constant of the graphite, we first consider a $\sqrt{3} \times \sqrt{3}R30^\circ$ commensurate overlayer with primitive

lattice vectors $\bar{R}_1 = 2\bar{a}_1 + \bar{a}_2$ and $\bar{R}_2 = \bar{a}_2 - \bar{a}_1$, where $\bar{a}_1 = a\hat{x}$ and $\bar{a}_2 = a/2(-\hat{x} + \sqrt{3}\hat{y})$ are the primitive lattice vectors of the substrate. The commensurate phase has lattice constant $|R_1| = |R_2| \equiv a_0 = \sqrt{3}a$. For such a lattice one out of three possible lattice sites on the substrate are occupied in any ordered region and consequently there are 3 types of domains. In the incommensurate phase we will assume that these domains are arranged so that they are connected by a hexagonal honeycomb of discommensurations (domain walls) which add $1/a'$ additional atoms per unit length with a' related to a_0 by a number of order unity that depends on the detailed structure of the walls. Such a structure is illustrated in Fig. 4. The free energy per unit area of the honeycomb incommensurate phase contains several terms. For the regular honeycomb array, the free energy ignoring wall-wall interactions is

$$f_R = \frac{2}{3\sqrt{3}l^2} \left[\frac{l}{a'} (\zeta_0 - \zeta) + 2f_l \right], \quad (3.1)$$

where f_l is the energy associated with each wall intersection and l is the length of one side of the hexagon.

In the limit of large separation of the walls (which we will assume henceforth) Villain⁹ has pointed out that the honeycomb array is degenerate in that one can "breathe" any hexagon, or group of hexagons, in or out without changing the total wall length or the number of intersections. This is illustrated in Fig. 1. The two configurations shown have the same number of intersections and the same wall length (due to the

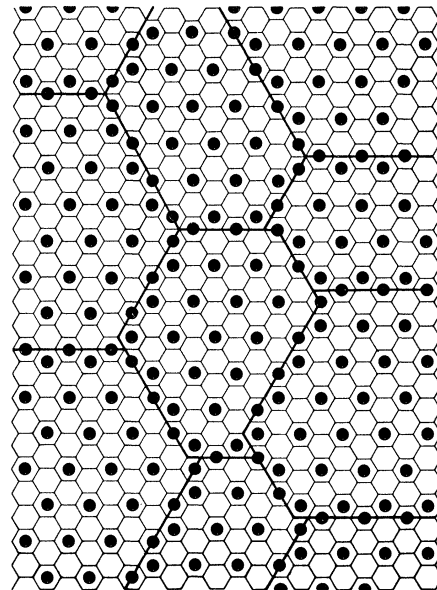


FIG. 4. Possible domain-wall structure for honeycomb discommensuration array.

120° intersection angles), and hence the same free energy. The number of possible “breathed” positions for a given hexagon is of order $(l/\bar{a})^B$ yielding an entropic contribution to the free energy per hexagon of the form $-BT \ln|l/\bar{a}|$, where B is a numerical constant, and $\bar{a} \sim a$.

We show below that B is in fact equal to one, and that to order l^{-2} the *only* contribution to the free energy not included in Eq. (3.1) arises from the entropy of breathing of rigid walls. In order to make this concept precise, let us assume that the allowed positions of the vertices are restricted to lie on the sites of a triangular lattice with lattice constant a . Then the entropy under consideration is simply the logarithm of the number of ways the vertices can be placed on the underlying lattice, and connected up with straight line segments parallel to the 120° axes, having the same *topology* as a regular honeycomb lattice of side l .

A lower bound for the entropy associated with breathing the honeycomb array is established as follows: Let each hexagon be “breathed” once, i.e., made larger or smaller (as in the Monte Carlo simulation discussed in Sec. III A), but only so that the change in position of the vertices of a given hexagon due to *its* breathing is less than $l/4$. It is clear that this restriction will ensure that the hexagons do not interfere with each others’ breathing. Since there are $l/2a$ possible configurations for each hexagon subject to this restriction, the entropy per hexagon is $\ln(l/2a)$, which is a lower bound of the desired form.

We now establish an upper bound. *Any* breathed configuration of the honeycomb is uniquely determined by specifying the *vertical* (y) coordinates of the vertices in alternate vertical zigzag columns (i.e., those vertices shown as solid dots in Fig. 5) and the horizontal position of just one dot in every column. The second part of this specification requires only $\sqrt{N_H}$ numbers for N_H hexagons and is hence negligible in the thermodynamic limit and can be ignored.

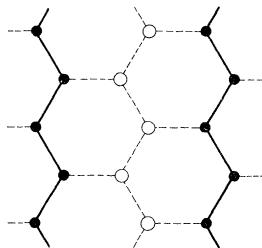


FIG. 5. Construct to obtain upper bound of entropy of hexagonal wall array and to show that the breathing freedom is dominant. Note that specifying the positions of the solid dots plus the position of only one unshaded dot per column specifies the array.

If all possibilities of the vertical positions of the solid dots in each column are allowed, regardless of whether or not the positions correspond to an allowed breathed configuration, but subject to the constraint that the average separation be l , then the resulting entropy (which is clearly an overestimate) can be shown to be $\ln(el/a)$ per hexagon (for $l/a \rightarrow \infty$). The desired result is thus proved by noting that $\ln(l/2a) < s < \ln(el/a)$, with s the breathing entropy per hexagon.

In addition to the above terms one must consider the effects of relaxing the rigid-wall constraints. In the large l limit, it can be shown that this does not give rise to extra terms in the free energy of order $\ln l$ per hexagon. The entropy of meandering of a single long wall is included in the free energy per unit projected length of the wall (i.e., the length projected onto the appropriate 120° axis). Thus we need only consider *changes* in this entropy. These may arise from (a) changes in the total projected wall length, (b) effective interaction between the walls due to collisions, and (c) constraints imposed by the honeycomb configuration. It is easy to see that even if the walls are allowed to meander and the vertices to move, the total “projected” length (which determines the number of extra atoms) of the walls remains unchanged, and hence (a) can be ignored. The effect of wall collisions (b) can also be neglected at large l as the resulting change in free energy is expected to be of order l^{-3} per unit area ($1/l$ per hexagon) by analogy with the striped phase discussed in the previous section. We are thus left with only the effects of the honeycomb constraints.

There is no loss of meandering entropy of the zigzag vertical walls (drawn as heavy lines in Fig. 5) caused by specifying the *vertical* positions of the solid vertices. This can be seen by considering the vertical walls to be walls meandering freely (up to the effects of other walls, see above), but with 120° changes in average direction at the solid vertices. These sudden changes in average direction will only affect the heavy walls in their immediate vicinity and hence cannot give rise to terms of order $\ln l$, although this effect will contribute to the wall crossing free energy, f_l .

The fluctuations of other walls we treat somewhat differently. A wall of length l with one end fixed will have fluctuations of order \sqrt{l} in the position of the other end. Fixing the second end will hence divide the number of configurations of the wall by a factor of order \sqrt{l} —resulting in a loss in the entropy of $1/2 \ln l$. For a given position of *all* the vertices, each of the $2N$ walls drawn dashed in the figure will thus have a loss of entropy of $1/2 \ln l$ giving an overall contribution to the entropy of $-N \ln l$. The N vertices with open circles will, however, each fluctuate in an area $(\sqrt{l})^2$ for a given position of the solid vertices. The contribution to the entropy from these

vertex fluctuations will hence be $+N \ln l$, exactly canceling the entropy loss of the light walls.

We have verified above that the *only* term of order $\ln l$ per hexagon arises from the counting of breathing configurations. Furthermore, the coefficient $B \equiv 1$ and $a/e < \bar{a} < 2a$. Given this result, the total free energy per unit area is

$$f = \frac{2}{3\sqrt{3}l^2} \left[\frac{l}{a'} (\zeta_0 - \zeta) + 2f_l - T \ln \left(\frac{l}{\bar{a}} \right) \right] + O\left(\frac{1}{l^3}\right). \quad (3.2)$$

For a given chemical potential, the equilibrium value of the average hexagon side length, l , is obtained by minimizing $f(l)$ with respect to l . There will be a C - I transition to the honeycomb phase at a critical value of the chemical potential, ζ_c , for which the minimum free energy from Eq. (3.2) becomes negative; i.e., lower than the free energy of the commensurate phase. As pointed out by Villain, this transition will be first order due to the effective attraction between the walls caused by the entropic contribution to the free energy. From Eq. (3.2), the critical chemical potential is

$$\zeta_c = \zeta_0 - \frac{a'}{l_c} T, \quad (3.3)$$

where l_c , the value of l at the C - I transition, is given by

$$l_c = \bar{a} e^{(1+2f_l/T)}. \quad (3.4)$$

We will assume that f_l is positive and several times larger than T , whence $l_c \gg a$. This implies that the walls are far apart at the transition—verifying our ansatz that terms in the free energy of order l^{-3} may be ignored. If, on the other hand, f_l were negative or $f_l \approx T$, the C - I transition would be strongly first order and little can be said in general. We will assume that this is *not* the case.

We now investigate the properties of the weakly incommensurate honeycomb phase with l large. At long wavelengths (much larger than l), the elastic free energy of the adsorbate may be written in terms of the displacements $\vec{u}(\vec{r})$ of the atoms from their average incommensurate positions:

$$F = \frac{1}{2} \int d^2r \left\{ \frac{\mu}{2} (\partial_i u_j + \partial_j u_i)^2 + \lambda (\vec{\nabla} \cdot \vec{u})^2 + \gamma (\vec{\nabla} \times \vec{u})^2 \right\}, \quad (3.5)$$

where we have assumed that the system of substrate plus adsorbate has mirror symmetry, and we assume that the displacements vanish at the boundary of the sample. The third term in (3.5), with elastic constant γ , arises from the lack of rotational symmetry due to

the substrate; the other terms depend on the usual Lamé coefficients, μ and λ . As for the striped phase, we may also write the free energy in terms of the wall displacements, $\vec{u}(\vec{r})$ and wall elastic constants $\tilde{\mu}$, $\tilde{\lambda}$, and $\tilde{\gamma}$. It will have exactly the same form as Eq. (3.5). The wall free energy will, in fact, have this form quite generally—even if, in the absence of mirror symmetry, the adsorbate free energy (in terms of the *atomic* displacements) is *more* complicated than Eq. (3.5) [i.e., there can be terms of form $(\vec{\nabla} \cdot \vec{u}) \times (\vec{\nabla} \times \vec{u})$]. All the results which are sensitive to long wavelengths may be calculated using either the adsorbate or the wall free energy, however; thus, for the above reason it is simpler (and more general) to work with the wall free energy.

For the simple highly symmetric type of walls shown in Fig. 4, the atomic displacements are related to the wall displacements by $\vec{u} = \vec{u}(a/\sqrt{3}l)$. This will not be true in general, however. The “bulk modulus,” $\tilde{\mu} + \tilde{\lambda}$, of the array of walls can be obtained from the variation of the free energy Eq. (3.2) with respect to the hexagon number density, $n = 2/(3\sqrt{3}l^2)$:

$$\tilde{\mu} + \tilde{\lambda} = n^2 \frac{\partial^2 f}{\partial n^2}. \quad (3.6)$$

Note that this is *not* the inverse compressibility since n is not generally proportional to the number of atoms per unit area. From Eqs. (3.2) and (3.3), one finds that at $\zeta = \zeta_c$

$$\tilde{\mu} + \tilde{\lambda} = \frac{T}{6\sqrt{3}l^2}. \quad (3.7)$$

As ζ increases, the product $l^2(\tilde{\mu} + \tilde{\lambda})$ increases monotonically, and for $\zeta = \zeta_0$ it is twice as large as at ζ_c .

The other elastic constants must be obtained by considering the effects of shear strains on the domain wall structure. First, we note that the breathing motion of the hexagons does not destroy any uniform imposed strain of the domain walls since this motion conserves the length of walls in all three directions. Therefore, we need only consider the possible strains of an array of regular hexagons. In any uniform strain all hexagons must distort in the same manner and therefore their opposite sides must be of equal length. The most general distortion is thus a combination of a compression and two pure shears. The two shears are illustrated in Fig. 6. Since these strains do not involve a rotation, $\tilde{\gamma}$ must be related to the energy to rotate the domain walls themselves. We can thus conclude that $\tilde{\gamma} \propto l^{-1}$ by analogy with \tilde{K}_y in the striped phase. Since $\tilde{\mu}$ and $\tilde{\lambda}$ are $\propto l^{-2}$, $\tilde{\gamma}$ may be taken to be infinite in the limit of large l .

The shear modulus, $\tilde{\mu}$, may be computed numerically by calculating the difference in breathing entropies

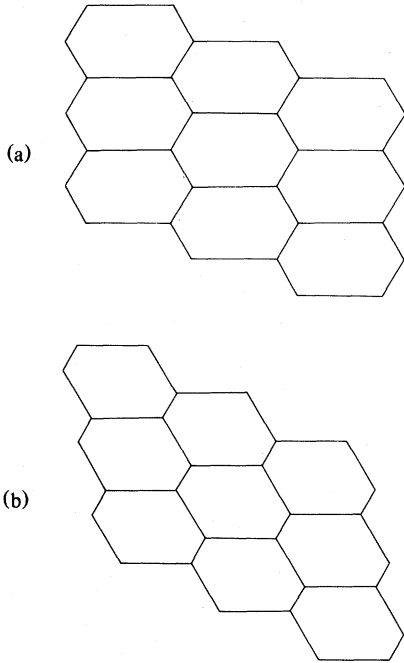


FIG. 6. Two pure shears that (together with a uniform compression) comprise the most general distortion of an array of identical hexagons.

py between a sheared and an isotropic array of hexagons. We have performed a Monte Carlo simulation of the honeycomb array and computed the entropy via an adaptation of a method used for hard spheres.¹⁸ This calculation is described in the next section. We find that $\tilde{\mu} = (0.5 \pm 0.1) T/l^2$. We note the peculiar result that $\tilde{\mu} > \tilde{\mu} + \tilde{\lambda}$, which implies that the system has a negative Poisson ratio—if the solid is squeezed along one axis, it shrinks in all directions. This occurs because the entropy of long thin hexagons is so much less than that of regular ones. The system resists shear in order to keep the hexagons as regular as possible.

Nelson and Halperin¹¹ have shown that any two-dimensional solid with an elastic free energy of the form Eq. (3.5) (in terms of the wall elastic constants) will be unstable to the presence of free dislocations with Burgers vector \tilde{b} if

$$\tilde{b}^2 \left(\tilde{\mu} \frac{(\tilde{\mu} + \tilde{\lambda})}{2\tilde{\mu} + \tilde{\lambda}} + \frac{\tilde{\mu}\tilde{\gamma}}{\tilde{\mu} + \tilde{\gamma}} \right) < 4\pi T. \quad (3.8)$$

The minimum allowed Burgers vector of the array walls which maintains the *ABC* domain labeling is $\tilde{b} = 3l$ corresponding to a dislocation in the adsorbate lattice with minimal Burgers vector, a_0 (see Fig. 7). Therefore, the lattice is unstable if the bracketed quantity is less than $4\pi T/9l^2$. Plugging in $\tilde{\gamma} = \infty$ and the calculated values of $\tilde{\mu}$ and $\tilde{\lambda}$ at $\zeta = \zeta_c$ one finds

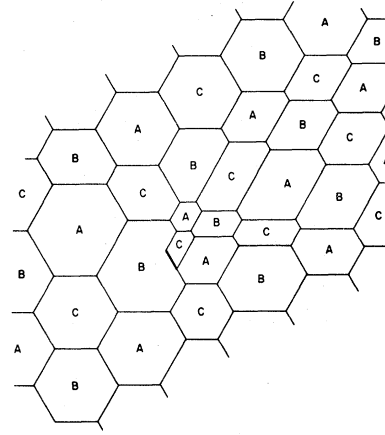


FIG. 7. An illustration of a dislocation in a $\sqrt{3} \times \sqrt{3} 30^\circ$ honeycomb structure.

that

$$\tilde{\mu} \left(\frac{(\tilde{\mu} + \tilde{\lambda})}{2\tilde{\mu} + \tilde{\lambda}} + 1 \right) = (5 \pm 1) T/9l^2 \leq 4\pi T/9l^2 \quad (3.9)$$

and hence the weakly incommensurate honeycomb phase is *unstable to dislocations and is necessarily a fluid at all temperatures.*

These results may be generalized to honeycomb incommensurate phases sufficiently near to other low-order commensurate phases, in a similar manner as with $p \times 1$ rectangular overlayers. With a the lattice constant of the graphite, we consider hexagonal commensurate overlayers with primitive lattice vectors $\tilde{\mathbf{R}}_1 = n\tilde{\mathbf{a}}_1 + m\tilde{\mathbf{a}}_2$ and $\tilde{\mathbf{R}}_2 = -m\tilde{\mathbf{a}}_1 + (n-m)\tilde{\mathbf{a}}_2$ where $\tilde{\mathbf{a}}_1 = a\hat{x}$ and $\tilde{\mathbf{a}}_2 = a(-1/2\hat{x} + \sqrt{3}/2\hat{y})$ are the primitive lattice vectors of the substrate. For such a lattice one out of $N = n^2 + m^2 - nm$ possible lattice sites on the substrate are occupied in any commensurate region and consequently there are N different domains or possible positions of the adsorbate array. The lattice constant a_0 of the commensurate phase (which equals the minimum microscopic Burgers vector) is

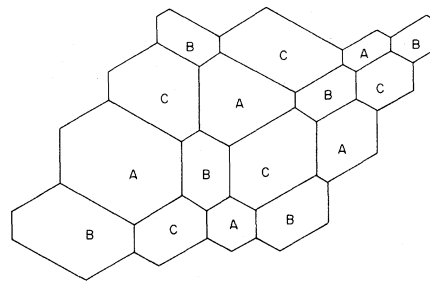


FIG. 8. Part of a "typical" configuration of hexagonal walls, obtained by repeatedly "breathing" a regular array.

$a\sqrt{N}$, and, assuming that the wall energies are such that all N domains are present, the minimum Burgers vector of the hexagonal array is $l\sqrt{3N}$. Thus when $[\tilde{\mu}(\tilde{\mu} + \tilde{\lambda})/(2\tilde{\mu} + \tilde{\lambda}) + \tilde{\mu}] \geq 4\pi T/3Nl^2$ (with $\tilde{\mu}$ and $\tilde{\lambda}$ the same as above), the incommensurate solid becomes stable. This occurs for overlayers for which $N \geq 7.5 \pm 1.5$. The accuracy of our calculation leave some uncertainty for $N = 7$ or 9.

A. Numerical calculation of the elastic constants

The coefficient $\tilde{\mu}$ must be calculated by numerically evaluating the free energy derivatives of a sheared array, of the type shown in Fig. 7. In order to find these derivatives, one needs an expression for the coefficient of the logarithmic entropy expression in Eq. (3.2) that can be evaluated numerically. We adapt a method used for hard spheres.¹⁸ We shall first describe a numerical procedure for calculating dS/dl .

Since the energy is constant for all configurations, it can be chosen to be zero, and one can write the partition function $Z = e^S$. Therefore, $dS/dl = d(\ln Z)/dl = Z^{-1} dZ/dl$. (We assume here that l is very large compared to the mesh-constant a .) The partition function Z is just the number of allowed configurations of the system. The derivative dZ/dl can be evaluated numerically by considering Z to be a function of $l - h$, an "available" length. Here, $h \ll l$ is the size of a "hard core" at the vertices. One can then count the number of configurations lost when the size of the core is increased. Since

$$\frac{dZ}{dl} = -\frac{dZ}{dh} \approx \lim_{h \rightarrow 0} \frac{Z(l, h) - Z(l, 0)}{h}, \quad (3.10)$$

$$\frac{dS}{dl} = \frac{d(\ln Z)}{dl} = \lim_{h \rightarrow 0} \frac{1}{h} \left[1 - \frac{\sum_{\omega \in \Omega(l)} X(h)}{\sum_{\omega \in \Omega(l)} 1} \right],$$

where $\Omega(l)$ is the set of allowed configurations with $h = 0$, and $X = 0$ for those configurations with any side length less than h and is 1 otherwise.

The quantity in brackets in (3.10) is just the probability that there is at least one side of length less than h in the original ensemble, or that there is an "overlap" between the vertices. Since the number of nodes is equal to the area A divided by $(3\sqrt{3}l^2/4)$, we have

$$\frac{l}{A} \frac{\partial S}{\partial l} = \left[\frac{2}{3l^2\sqrt{3}} \right] \lim_{h \rightarrow 0} \bar{B}(h/l), \quad (3.11)$$

where

$$\bar{B}(h/l) \equiv \left\langle \frac{2l}{h} \left\langle \frac{N_o}{N_n} \right\rangle \right\rangle, \quad (3.12)$$

where N_o is the number of overlaps and N_n is the

number of nodes. This last step assumes that the probabilities of the walls having lengths less than h are independent for small h ; although it is not altogether obvious that this assumption holds, the close agreement between numerical calculation and the analytic result as $h \rightarrow 0$ indicates that the procedure is valid. It is easy to see that in the limit, $h/l \rightarrow 0$, the quantity $\bar{B}(h/l)$ equals the coefficient B defined in Sec. III.

The shear modulus, $\tilde{\mu}$, is calculated by finding the entropy of an array generated from the lattice pictured in Fig. 6(a). The regular lattice is distorted slightly by making the sides parallel to \hat{x} ("horizontal" sides) length $l(1 + \epsilon)$ and the other sides length $l(1 - \epsilon/2)$. The resulting array has to first order in ϵ the same area and the same energy as a regular array of the same number of regular hexagons with side l . The strains in this array are

$$\tilde{u}_{yy} = -\tilde{u}_{xx} = \frac{\epsilon}{2}, \quad \tilde{u}_{xy} = \tilde{u}_{yx} = 0. \quad (3.13)$$

The definition of the Lamé coefficients then implies $\Delta F = \epsilon^2 \tilde{\mu}/2$. For an array with a fixed number of hexagons, since the total length of wall remains constant, the only change in the total free energy is due to changes in the entropy of the configuration, which is calculated below. However, since the free energy must be calculated to $O(\epsilon^2)$, it is necessary to note that in this order the area of each hexagon is reduced, so the change in the free energy per unit area [to $O(\epsilon^2)$] is

$$\delta(F/A) = -\frac{F}{A^2} \delta A + \frac{\delta F}{A}. \quad (3.14)$$

However, at the I - C transition $F = 0$ and the first term of this expression may be ignored. Therefore, one need only consider changes in the entropy;

$$\Delta F = -T \left[\epsilon \left. \frac{\partial S}{\partial \epsilon} \right|_{\epsilon=0} + \frac{1}{2} \epsilon^2 \left. \frac{\partial^2 S}{\partial \epsilon^2} \right|_{\epsilon=0} \right]. \quad (3.15)$$

Defining $l_1 = l(1 + \epsilon)$ and $l_2 = l(1 - \epsilon/2)$, one obtains

$$\Delta F = -T \left[\epsilon l \left[\left. \frac{\partial S}{\partial l_1} - \frac{1}{2} \frac{\partial S}{\partial l_2} \right]_{\epsilon=0} + \frac{1}{2} \epsilon^2 l \frac{\partial}{\partial \epsilon} \left[\left. \frac{\partial S}{\partial l_1} - \frac{1}{2} \frac{\partial S}{\partial l_2} \right]_{\epsilon=0} \right] \right]. \quad (3.16)$$

As derived above,

$$\frac{l}{A} \frac{\partial S(h, l)}{\partial l} = \lim_{h \rightarrow 0} \frac{4}{3\sqrt{3}l^2} \frac{l}{h} \left[\frac{N_l}{N_n} \right],$$

where N_l is the number of sides with length $< h$. There are half as many horizontal sides as vertical

sides, so by symmetry

$$\left(\frac{\partial S}{\partial l_1} - \frac{1}{2} \frac{\partial S}{\partial l_2} \right)_{\epsilon \rightarrow 0} = 0 \quad (3.17)$$

Therefore, as expected, only the ϵ^2 term contributes to the free energy, and

$$\Delta F = \lim_{\epsilon \rightarrow 0} -T \frac{1}{2} \frac{\epsilon^2 l}{\epsilon} \left[\left(\frac{\partial S}{\partial l_1} - \frac{1}{2} \frac{\partial S}{\partial l_2} \right)_{l_1=l(1+\epsilon), l_2=l(1-\epsilon/2)} - \left(\frac{\partial S}{\partial l_1} - \frac{1}{2} \frac{\partial S}{\partial l_2} \right)_{l_1=l_2=l} \right] \quad (3.18)$$

The second term is again zero by symmetry, so

$$\Delta F = \lim_{\epsilon \rightarrow 0} \left[-\frac{1}{2} \epsilon l T \left(\frac{\partial S}{\partial l_1} - \frac{1}{2} \frac{\partial S}{\partial l_2} \right)_{l_1=l(1+\epsilon), l_2=l_2(1-\epsilon/2)} \right] \quad (3.19)$$

and

$$\tilde{\mu} = \frac{4}{3\sqrt{3}} \frac{T}{l^2} \frac{1}{\epsilon} \frac{1}{h} \frac{1}{N_n} \left(\frac{1}{2} N_v - N_h \right), \quad (3.20)$$

where N_v is the number of vertical sides $< h$ and N_h the number of horizontal sides $< h$.

The arrays used for the calculations were generated from arrays of identical hexagons similar to the ones pictured in Figs. 1 and 6(a). It was found that using coordinate axes oriented at 120° angles (parallel to two of the three wall directions) made the calculations simpler. The system was symmetrically placed with the axes, i.e., its overall shape was that of a parallelogram with included angles of 60° and 120° and its sides perpendicular to the axes. Periodic boundary conditions were imposed between the parallel sides of the array.

The Monte Carlo calculation was implemented by repeatedly choosing a hexagon at random, and changing its size according to the following procedure. The six vertices of the chosen hexagon are moved in or out along the six 120° directions by equal distances $|s|$, where we take $s > 0$ to denote expansion and $s < 0$ to represent contraction of the hexagon. In order to choose s , we first determine the maximum possible expansion ($s_{\max} \geq 0$) and the maximum possible contraction ($s_{\min} \leq 0$) of the chosen hexagon, consistent with the constraint that the honeycomb topology be preserved. The expansion distance s is then chosen to be a random number, uniformly distributed between s_{\min} and s_{\max} . In principle s should be an integral multiple of the underlying mesh constant a ; however we have taken the continuum limit, $a/l \rightarrow 0$.

It is easy to check that this described procedure satisfies detailed balance—i.e., if α and β are two allowed configurations of the vertices, the probability of making a transition from α to β is the same as the probability of making a transition from β to α .

Furthermore, any configuration of the system can be reached from any other, in a finite number of steps. It follows that in the limit of a large number of Monte Carlo steps, we approach an equilibrium distribution, in which the probability of finding any allowed configuration is the same as any other. Part of a “typical” configuration is shown in Fig. 8.

The calculation of the entropy was done by repeatedly “breathing” the array and counting the number of side lengths less than a given value. The results were then averaged. The quantity $\bar{B}(h/l)$ was then determined from Eq. (3.12). Equilibrium was tested by the convergence of the Lamé coefficient calculations.

A typical run involved a 70×70 array. After 147 000 “breathing” motions (30 per hexagon), the entropy per hexagon was calculated. After an additional 30 motions, it was again calculated, until 166 values were obtained. These data were averaged and the resulting values of \bar{B} plotted in Fig. 9. It is found that \bar{B} varies about 10% between $h=0$ and $h=l/10$, which indicates that there is some correlation between side lengths. However, the limit as $h \rightarrow 0$ gives the correct value $B = 1.00 \pm 0.01$, in good agreement with the analytic result.

The calculations of the Lamé coefficient $\tilde{\mu}$ was done by “breathing” a sheared array like that pictured in Fig. 6(a). After every 100 breathing motions per hexagon the right-hand side of Eq. (3.14) was calculated for various h and used to calculate $\tilde{\mu}$. After 350 averages of both a 30×30 and a 40×40 array, the data shown in Fig. 10 were obtained.

For the range of h/l used, the numerically calculated \bar{B} stays within 5% of the value 1, so the error induced by considering the side lengths as totally independent is much less than the scatter of the data. The slow convergence of the results for $\tilde{\mu}$ is expected because Eq. (3.20) is the difference of two comparatively large numbers and hence exhibits large random

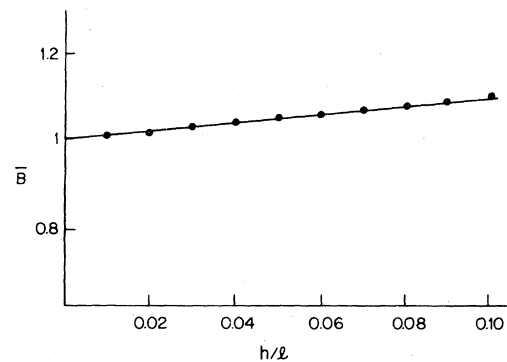


FIG. 9. Numerical calculation of $B = l/h \{S(l) - S(l-h)\}$, where S is the entropy per hexagon and l is the average side length of a hexagon. As expected, as $h/l \rightarrow 0$, $B \rightarrow 1$.

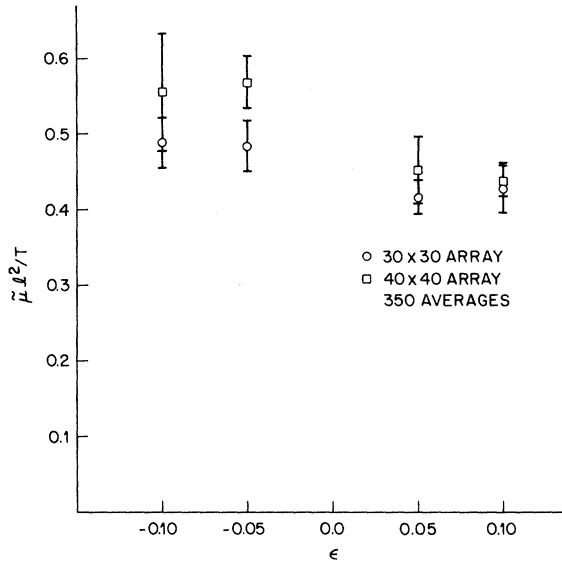


FIG. 10. Numerical calculation of $\tilde{\mu}$ using Eq. (3.14). ϵ measures the shear of the array, and $\tilde{\mu}$ is determined by the free energy change for a given shear.

fluctuations. The running time of the program therefore becomes a major limitation. From these data, we have concluded that

$$\tilde{\mu} = \frac{T}{l^2} (0.5 \pm 0.1) . \quad (3.21)$$

As expected, $\tilde{\mu}$ is more or less independent of $\epsilon, h/l$, and the array size, for reasonable choices of the parameters.

A check on these results was attempted using the correlation function calculation outlined in the Appendix. This last calculation converged very slowly; however, an upper bound of $2\tilde{\mu} + \tilde{\lambda} \leq 0.7T/l^2$ was obtained, which is consistent with the above results.

IV. HONEYCOMB TO STRIPED TRANSITION

For $\zeta_c < \zeta < \zeta_0$, the honeycomb phase will be the lowest free energy phase. When $\zeta > \zeta_0$, however, we must directly compare the energies of the honeycomb and the striped phases. For $\zeta - \zeta_0 \leq |\zeta_c - \zeta_0|$, l will be of order l_c , and the honeycomb free energy will be a weak function of $\zeta - \zeta_0$

$$f_H \sim \frac{\zeta_c - \zeta_0}{l_c} \sim -Te^{-4f_l/T} .$$

(We will ignore all microscopic lengths; l will be measured in units of these.)

The striped phase free energy, on the other hand

depends strongly on $\zeta - \zeta_0$,

$$f_s \sim -[\Gamma(\zeta - \zeta_0)^3/T^2]^{1/2} .$$

There will thus be a first-order transition from the honeycomb to the striped phase at a value of the chemical potential given by

$$\zeta_{HS} - \zeta_0 \sim e^{-8f_l/3T} (T^2/\sqrt{\Gamma})^{2/3} .$$

On the scale of chemical potential set by $\zeta_0 - \zeta_c \sim Te^{-2f_l/T}$, $\zeta_{HS} - \zeta_0$ is exponentially small; i.e., the honeycomb-striped transition will occur extremely near ζ_0 . The wall separation in the striped phase at the transition will be

$$l_s \sim l_c^{2/3} (T/\Gamma)^{1/3} ,$$

which is much smaller than in the honeycomb phase at ζ_{HS} , $l_H \approx l_c/\sqrt{e}$. The jump in particle density will thus be considerably larger at the honeycomb-striped transition than at the commensurate-honeycomb-incommensurate transition.

We note that the presence of free dislocations in the honeycomb phase will lower its free energy somewhat and may perhaps make the honeycomb $C-I$ transition second order. However, since the number of dislocations will be thermally activated, the above analysis will be valid at low temperatures if the dislocation core energy is sufficiently large. (In this limit the honeycomb $C-I$ transition will still be first order.) In particular, for $p = N = 3$, there will be a transition at $\zeta_{HS} \approx \zeta_0$ from an isotropic fluid to an anisotropic (striped) solid.

As the chemical potential is increased from ζ_{HS} , the striped phase will become more and more anisotropic as l decreases. At some critical value of l (comparable to the width of an isolated domain wall), the adsorbate will generally revert back to an isotropic hexagonal solid. This will almost certainly occur unless the substrate-adsorbate potential is very large, so that the domain walls are very narrow.

A. Rotated phases

Up to this point, we have assumed that the domain walls are parallel to the crystalline axes of the substrate (which for the following discussion we will take to be hexagonal). In fact, this will not always be the case. We will discuss below the effects, near the $C-I$ transition, of instabilities which cause the walls to rotate.

Novaco and McTague¹³ have calculated the total energy at $T=0$ as a function of the relative angle of the adsorbate and substrate crystalline axes in the limit that the substrate potential is weak. They find that if the microscopic Lamé coefficient λ_0 of the adsorbate is positive (which it will be for almost all real substances), the energy is minimum for a nonzero

value of the angle. Villain¹⁹ and Pokrovskii²⁰ have shown that in the domain wall limit (i.e., near to the $C-I$ transition at a fixed magnitude of the substrate potential) the minimum energy is realized if the walls are tilted at a finite angle θ_0 . While the criteria in terms of microscopic parameters may generally be different in this limit, the result is the same: a relative rotation of the adsorbate and substrate axes by an angle which tends to zero as l^{-1} for $l \rightarrow \infty$. This picture, which has been verified experimentally, must be modified in the presence of thermal fluctuations.

We first consider a single wall which we will assume to be rotated away from a substrate axis by an angle θ_0 , which we can take to be $< 30^\circ$. At any nonzero temperature the wall will not be straight but will have two kinds of fluctuations. First, as for walls with $\theta_0 = 0$, there will be small glitches in the wall position which will give rise to slow meandering about the average direction, θ_0 . Secondly, however, there may be sudden changes in the wall direction, from θ_0 to $-\theta_0$, which will cost some microscopic energy f_B . Bends from θ_0 to $\theta_0 \pm 60^\circ$, which might be expected to be important will, on the other hand, cost an energy proportional to the length of the bent section and hence will not play a role, except to contribute to the slow meandering. At low temperatures, the distance, between bends from θ_0 to $-\theta_0$ (or vice versa) will be $y_B \propto e^{-f_B/T}$. A single long wall will, due to these bends, always on average have no rotation away from $\theta = 0$. However, the meandering will be dominated by the large excursions between bends. The "diffusion constant" of the wall will hence diverge as $T \rightarrow 0$, $T/\Gamma \propto e^{f_B/T}$. The striped phase near to the second order $C-I$ transition will not be rotated, since at any fixed T , sufficiently close to the transition l will be much larger than y_B and the discussion in Sec. II will apply. When l decreases to be of order y_B , there will be a transition to a rotated striped phase in which all walls are inclined with a mean angle $\approx \theta_0$.

Even though the adsorbate long wavelength free energy of this rotated striped phase need not be of the form Eq. (2.10), the wall free energy will still be of the form Eq. (2.7) as long as $l \gg a$. The instability analysis of the striped phase can hence be carried over trivially to the rotated case in the limit $y_B \gg l$. Near the rotational transition, the elastic constants will not be simply related to each other and the details of the analysis do not apply.

For the honeycomb case, the situation is somewhat different. The relevant length scale is now that of the first-order $C-I$ transition, $l_c \propto e^{2f_l/T}$. If $l_c \gg y_B$ (i.e., $2f_l \gg f_B$), the honeycomb phase will not be rotated near the transition and the analysis in Sec. III will apply. If $a \ll l_c \ll y_B$ on the other hand, the honeycomb will be rotated by θ_0 with respect to the substrate. Again, while the adsorbate long-wavelength free energy will be complicated, the wall

free energy will have the same form as for the nonrotated phase, and the arguments in Sec. III will apply.

In the intermediate case, $l_c \sim y_B$, the situation will be more complicated. We note only here that, in contrast to the striped phase, there cannot be a nonrotated to rotated phase transition (as a function of chemical potential) within the honeycomb phase in a regime of the phase diagram in which the calculations in this paper apply. This is due to the narrow range of l for which the honeycomb phase is stable (see above). We cannot, of course, rule out a rotational phase transition far from the $C-I$ transition where the details of the wall-wall interactions are important. Rotational instabilities and the effects of thermal fluctuations upon them will be discussed in detail in a future paper.

V. DISCUSSION OF EXPERIMENTS ON KRYPTON ON GRAPHITE

Various low-energy electron diffraction (LEED)⁴ and x-ray scattering^{2,3} studies of krypton physisorbed on grafoil have shown that as a function of chemical potential and temperature, krypton monolayers exhibit several phases including a $\sqrt{3} \times \sqrt{3}$ commensurate solid, an isotropic incommensurate solid phase, and a fluid phase. The "natural" lattice spacing of the krypton (i.e., the close-packed lattice spacing at $T = 0$ on a smooth substrate), is 7% less than $\sqrt{3}$ times the distance between graphite adsorption sites, making krypton on graphite a natural system for studying the $C-I$ transition from a $\sqrt{3} \times \sqrt{3}$ hexagonal registered phase.

Very recently, Moncton *et al.*³ have studied the $C-I$ transition via very high-resolution x-ray scattering, at temperatures $T \approx 80$ K, considerably lower than the ~ 110 -K melting temperature of the incommensurate solid obtained from adsorption isotherms. They observe a second-order (or weakly first-order) transition from a commensurate solid with a correlation length of ~ 2500 Å to a fluid phase with a rather long correlation length of order hundreds of angstroms. The fluid phase is observed to be incommensurate in the sense that the peak in $S(q)$ moves smoothly away from the commensurate position (G_c) to higher values of $q = G_c + \epsilon$. The correlation length (inverse width) initially decreases roughly in proportion to the peak shift; however, as the incommensurability increases, the peak sharpens up again—presumably $S(q)$ has acquired the form appropriate to a two-dimensional floating solid. It is natural to interpret the existence of a narrow fluid phase down to at least 80 K as support for the results of this paper. However, as will be discussed below, the connection between the theory and the experimental results of Moncton *et al.* is at best suggestive.

The modulation in the krypton-graphite potential, as a function of position in the xy plane, is believed to be about 40 K, which should be compared with the 150-K minimum in the attractive interaction between the krypton atoms. This relatively weak substrate potential and the hard core repulsions between the krypton atoms suggest that the domain walls in the weakly incommensurate phase will be reasonably broad—a fact which complicates considerably the possible interpretation of the experiments in terms of the concepts discussed in this paper.

In addition to the peak in $S(q)$ at $G_c + \epsilon$, Moncton *et al.*³ observe a considerably smaller peak at $G_c - \epsilon/2$ caused by modulation of the krypton by the graphite. At zero temperature, in the limit that the distances between the walls are much larger than the wall width, the peak at $G_c - \epsilon/2$ would be expected to have twice the intensity (in a powder average) of the peak at $G_c + \epsilon$. If, on the other hand, the modulation of the krypton by the graphite is weak, the peak at $G_c - \epsilon/2$ would be smaller than that at $G_c + \epsilon$. In the absence of any calculations in either limit for $S(q)$ at finite temperatures, it is not possible to decide whether the measured relative intensity of the two peaks is more consistent with a domain wall or a weakly modulated structure. In either case, the details of our calculation probably do not apply in the region of the phase diagram studied thus far with high resolution. It seems plausible, however, that in a narrow range of chemical potential at sufficiently low temperatures the domain wall description may be valid. The reason for the observed depression of the melting temperature may then be directly related to the softening of the weakly incommensurate krypton lattice caused by fluctuations of the positions of the higher density regions of the system, analogous to the “breathing modes” which we have studied here in the limit of well separated domain walls.

It should be mentioned here that several alternate explanations have been proposed for the observed broadening of the Bragg peak near the commensurate-incommensurate transition. For example, it has been noted that at $T = 0$ (or in mean-field theory) there exist at least metastable “chaotic” states near the commensurate-incommensurate transition in

which domain walls occur with a pseudorandom spacing, which would cause translational correlations to fall off exponentially with distance, even though the adsorbate lattice is free of dislocations.²¹ It is not clear, however, that such states will correspond to a state of minimum energy at $T = 0$, or that such chaotic states would be stable at temperatures different from zero. Furthermore, if a chaotic state could otherwise exist at $T \neq 0$, it would appear to have a vanishing macroscopic elastic constant. It follows that such a state should be unstable to the formation of free dislocations, in two dimensions, and therefore would actually be a liquid.

Villain²² has pointed out that the dilute domain-wall structure is easily distorted by defects in the substrate surface, and that the energy gained by such distortions may in practice have an important effect on the commensurate-incommensurate transition. Substrate defects could also be responsible for the broadening of the Bragg peaks. These possibilities can best be explored by further experiments on a variety of surfaces.

ACKNOWLEDGMENTS

The authors acknowledge several stimulating discussions with D. E. Moncton, R. J. Birgeneau, and S. Ostlund. We also acknowledge several helpful reports of unpublished work from J. Villain. The work at Harvard was supported in part by NSF Grant No. DMR 77-10210.

APPENDIX

The calculation of the elastic constants for the honeycomb phase can be checked by calculating the correlation function in the long-wavelength limit. After defining the Fourier transform of the displacement field,

$$\bar{u}(\vec{q}) = \frac{1}{\sqrt{N}} \sum_i e^{-i\vec{q} \cdot \vec{R}_i} \bar{u}(\vec{R}_i) \quad (A1)$$

The correlation function is

$$\langle \bar{u}(\vec{q}) \bar{u}(-\vec{q}) \rangle = \frac{\int e^{-\beta H(\bar{u}(\vec{q}))} \bar{u}(\vec{q}) \bar{u}(-\vec{q}) \prod_Q d^2 u(Q)}{\int e^{-\beta H(\bar{u}(\vec{q}))} \prod_Q d^2 u(Q)} \quad (A2)$$

In this expression $\beta = 1/T$ and H is the elastic free energy Eq. (3.5) written in terms of the $\bar{u}(\vec{q})$.

$$H = \frac{1}{2\rho} \sum_Q \left[\frac{\mu}{2} |q_i u_j + q_j u_i|^2 + \lambda [\vec{q} \cdot \bar{u}(\vec{q})]^2 + \gamma (\vec{q} \times \bar{u})^2 \right] = \frac{1}{2\rho} \sum_Q \left[(2\mu + \lambda) q^2 u_{\parallel}^2(\vec{q}) + (\mu + \gamma) q^2 u_{\perp}^2(\vec{q}) \right] \quad (A3)$$

Here $u_{\parallel}(\vec{q})$ and $u_{\perp}(\vec{q})$ are the components of $\bar{u}(\vec{q})$ parallel and perpendicular to \vec{q} . Inserting this expression into Eq. (A2) we find

$$\begin{aligned} \langle u_{\parallel}(\vec{q})u_{\parallel}(-\vec{q}) \rangle &= \frac{\rho T}{(2\mu + \lambda)q^2}, \\ \langle u_{\perp}(\vec{q})u_{\perp}(-\vec{q}) \rangle &= \frac{\rho T}{(\mu + \gamma)q^2}. \end{aligned} \quad (\text{A4})$$

Since γ is infinite in the approximation of stiff walls we expect $q^2 \langle u_{\perp}(\vec{q})u_{\perp}(-\vec{q}) \rangle$ to go to zero as q becomes small. On the other hand $q^2 \langle u_{\parallel}(\vec{q})u_{\parallel}(-\vec{q}) \rangle$ should give $(2\mu + \lambda)$ as q becomes small. The calculation of the correlation functions $\langle \bar{u}_{\parallel}(\vec{q})\bar{u}_{\parallel}(-\vec{q}) \rangle$ and $\langle \bar{u}_{\perp}(\vec{q})\bar{u}_{\perp}(-\vec{q}) \rangle$ was performed for a microscopic adsorbate array with the wall structure pictured in Fig. 4. The $\bar{u}(\vec{R}_i)$ are defined to be the displacements between the positions of the atoms in the actual array (with walls) and their location in a perfect incommensurate array, i.e., one with the same net density but on a perfectly smooth substrate. The \vec{R}_i is thus the position of the i th atom in a perfect incommensurate array and $\vec{R}'_i = \vec{R}_i + \bar{u}(\vec{R}_i)$ is the actual position of atom i .

After choosing the origin to have the same position in the walled incommensurate and perfect incommensurate phases, it is straightforward to calculate $\bar{u}(\vec{R}_i)$ for a given \vec{R}_i in the walled array. [The choice of origin is unimportant because the interesting quantity is $\bar{u}(\vec{q})$. The actual algorithm subtracts the value of $\bar{u}(\vec{R}_i)$ at the centers of a regular array to simplify the formulas, but the choice in the text is conceptually simpler.] First, the number of walls

$$\bar{u}(\vec{q}) = \frac{1}{\sqrt{N}} \sum_{h \text{ hexagons}} e^{i\vec{q} \cdot \vec{R}_h} \sum_{i \in h} e^{i\vec{q} \cdot (\vec{R}'_i - \vec{R}_h)} [\bar{u}(\vec{R}_h) + \bar{u}(\vec{R}_i) - \bar{u}(\vec{R}_h)],$$

where \vec{R}_h is the position in the perfect incommensurate phase of the atom at the center of the distorted hexagon h :

$$\vec{R}_h \sum_{i \in h} 1 = \sum_{i \in h} \vec{R}_i.$$

Since $\vec{R}_i - \vec{R}_h$ is of order l , the exponential may be expanded in the long-wavelength limit ($ql \ll 1$), to yield

$$\bar{u}(\vec{q}) = \frac{1}{\sqrt{N}} \sum_h e^{i\vec{q} \cdot \vec{R}_h} \sum_{i \in h} [1 + i\vec{q} \cdot (\vec{R}_i - \vec{R}_h) + O(q^2)] \{\bar{u}(\vec{R}_h) + [\bar{u}(\vec{R}_i) - \bar{u}(\vec{R}_h)]\}.$$

Since

$$\bar{u}(\vec{R}_i) - \bar{u}(\vec{R}_h) \propto \vec{R}_i - \vec{R}_h, \quad \text{and} \quad \sum_{i \in h} (\vec{R}_i - \vec{R}_h) = 0,$$

we have

$$\bar{u}(\vec{q}) = \frac{1}{\sqrt{N}} \sum_h e^{i\vec{q} \cdot \vec{R}_h} \sum_{i \in h} [\bar{u}(\vec{R}_h) + O(ql)] = \frac{1}{\sqrt{N}} \sum_h e^{i\vec{q} \cdot \vec{R}_h} \bar{u}(\vec{R}_h) \frac{A_h}{(\sqrt{3}a^2/2)} + O(ql),$$

where A_h is the area of hexagon h . Thus, it is only necessary to find the area of each hexagon and the location of its center to calculate $\bar{u}(\vec{q})$ for small q .

The averages $\langle \bar{u}_{\parallel}(\vec{q})\bar{u}_{\parallel}(-\vec{q}) \rangle$ and $\langle \bar{u}_{\perp}(\vec{q})\bar{u}_{\perp}(-\vec{q}) \rangle$ were calculated for many configurations,

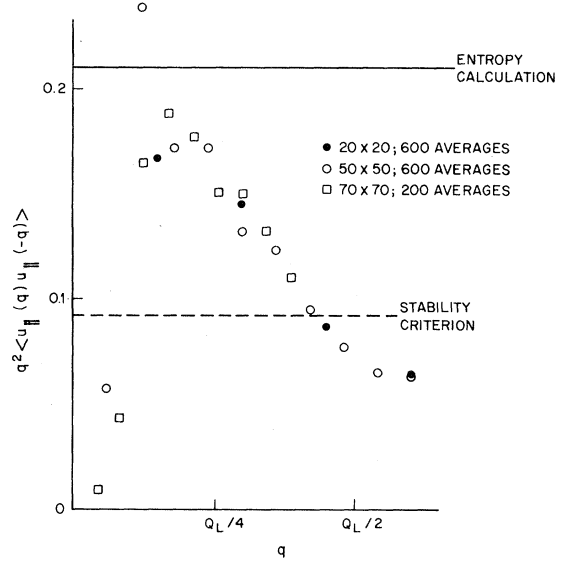


FIG. 11. Plot of longitudinal correlation function.

between the origin and \vec{R}'_i is found and a displacement of $a_0/\sqrt{3}$ perpendicular to each of these walls is added to yield the position of atom i . The vector \vec{R}_i is then this result scaled by the factor a'_0/a_0 , and $\bar{u}(\vec{R}_i) = \vec{R}_i - \vec{R}'_i$. Here $a'_0 = a_0/(1 + a_0/3l)$ is the incommensurate lattice constant.

The Fourier transform $\bar{u}(\vec{q})$ can now be calculated; the sum in Eq. (A1) simplifies for small q . We write

with various values of \vec{q} on the Γ line, i.e., in the direction of the zone corner, $Q = 4\pi/3\sqrt{3}l$. The results of several runs are plotted in Fig. 10. For example, the correlation function for 4900 hexagons was calculated every 147 000 "breathing"

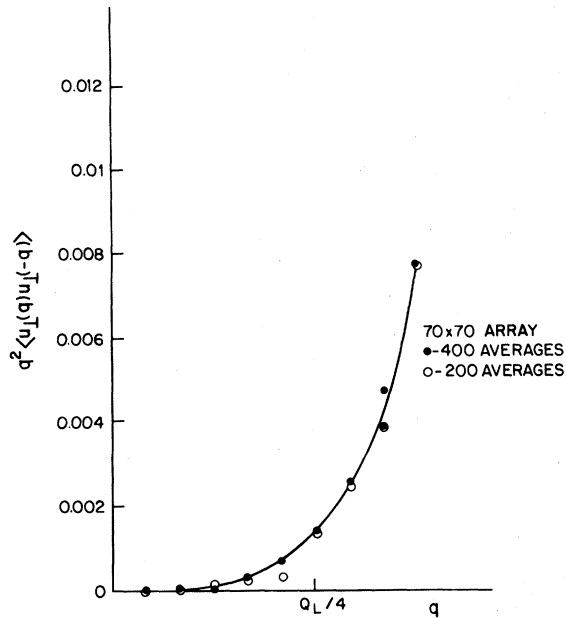


FIG. 12. Transverse correlational function. Note the extremely small values indicative of $\gamma = \infty$.

motions (30 per hexagon) up to a total of 29 440 000 motions (200 averages) to yield the squares in Fig. 11. The convergence at small wavelengths is very slow. The lack of equilibrium of the long-wavelength modes causes the first few data points to be anomalously low (though as the running time is increased this effect becomes less marked). In addition, the long-wavelength approximation seems to break down at q values of about $Q/4$. It is hence very difficult to extract a reliable value of μ . However, it seems quite clear that the correlation function yields a shear modulus much lower than that bound necessary for stability to dislocation formation. The values calculated in the text of $\tilde{\mu} = (0.5 \pm 0.1) T/l^2$ and $\tilde{\mu} + \tilde{\lambda} = T/6\sqrt{3}l^2$ correspond to $q^2 \langle u_{\parallel}(q)u_{\parallel}(-q) \rangle = \rho T/(2\mu + \lambda) = 0.21 \pm 0.3$, which as shown in Fig. 11, is reasonably consistent with the results of this calculation.

The transverse correlation function $\langle \bar{u}_{\perp}(\bar{q})\bar{u}_{\perp}(\bar{q}) \rangle$ was also calculated. Since it is proportional to $T/(\mu + \gamma)$, and $\gamma = \infty$, one expects that $q^2 |\bar{u}_{\perp}(\bar{q})|^2$ should go to zero at small q . Note that, as expected, the correlation function does not diverge as $q \rightarrow 0$. The results of the calculations are shown in Fig. 12.

*Present address: Physics Dept., Cornell University, Ithaca, N.Y. 14853.

¹See, for example, in *Ordering in Two Dimensions*, edited by S. K. Sinha (North-Holland, New York, 1980).

²P. M. Horn, R. J. Birgeneau, P. Heiney, and E. M. Hammonds, *Phys. Rev. Lett.* **41**, 461 (1978).

³D. E. Moncton, P. W. Stephens, R. J. Birgeneau, P. M. Horn, and G. S. Brown, *Phys. Rev. Lett.* **46**, 1533 (1981); see also articles in Ref. 1.

⁴M. D. Chinn and S. C. Fain, Jr., *Phys. Rev. Lett.* **39**, 146 (1977).

⁵W. L. McMillan, *Phys. Rev. B* **14**, 1496 (1976).

⁶P. Bak and V. J. Emery, *Phys. Rev. Lett.* **36**, 978 (1976).

⁷V. L. Pokrovskii and A. L. Talapov, *Phys. Rev. Lett.* **42**, 65 (1979).

⁸A. Luther and V. L. Pokrovskii (unpublished).

⁹J. Villain, in *Ordering in Strongly Fluctuating Condensed Matter Systems*, edited by T. Riste (Plenum, New York, 1980), p. 221.

¹⁰J. M. Kosterlitz and D. J. Thouless, *J. Phys. C* **6**, 1181 (1973).

¹¹D. R. Nelson and B. I. Halperin, *Phys. Rev. B* **19**, 2457 (1979).

¹²H. J. Schulz, *Phys. Rev. B* **22**, 5274 (1980). See also Ref. 9.

¹³A. D. Novaco and J. P. McTague, *Phys. Rev. Lett.* **38**, 1286 (1977); *J. Phys. (Paris)* **38**, C4-116 (1977).

¹⁴S. N. Coppersmith, D. S. Fisher, B. I. Halperin, P. A. Lee, and W. F. Brinkman, *Phys. Rev. Lett.* **46**, 549 (1981); **46**, 869(E) (1981).

¹⁵J. Villain and P. Bak, *J. Phys. (Paris)* (in press). See also, S. Ostlund (unpublished).

¹⁶S. T. Chui, *Phys. Rev. B* **23**, 5982 (1981).

¹⁷J. Villain, see Ref. 1.

¹⁸H. Reiss, H. L. Frisch, and J. L. Lebowitz, *J. Chem. Phys.* **31**, 369 (1959).

¹⁹J. Villain, *Phys. Rev. Lett.* **41**, 36 (1978).

²⁰V. L. Pokrovskii (unpublished).

²¹S. Aubry, in *Solitons and Condensed Matter Physics*, edited by A. R. Bishop and T. Schneider (Springer, Berlin, 1978), p. 264; P. Bak (unpublished); E. Fradkin and B. A. Humberman (unpublished).

²²J. Villain, *J. Phys. (Paris) Lett.* **41**, L267 (1980).